Energy efficient design of membrane processes by use of entropy production minimization

Elisa Magnanelli[a,*], Øivind Wilhelmsen[b,c], Eivind Johannessen[a], Signe Kjelstrup[a]

[a] *Department of Chemistry, NTNU - Norwegian University of Science and Technology, N-7491 Trondheim, Norway*
[b] *Department of Energy and Process Engineering, NTNU - Norwegian University of Science and Technology, N-7491 Trondheim, Norway*
[c] *SINTEF Energy Research, N-7465 Trondheim, Norway*

Abstract

To minimize entropy production means to reduce the lost work in a process, and to optimize the use of energy resources. Due to the need for re-compression, membrane units for separation of CO_2 from natural gas require large amounts of electrical power. We show that this power requirement can be reduced by controlling the permeation process so that the entropy production is minimum. With the use of optimal control theory, we develop in this work a detailed and robust method to minimize the entropy production of a membrane unit for separation of CO_2 from natural gas, by control of the partial and total pressures on the permeate side. Moreover, we show how the continuous optimal results can serve as ideal limits for the practical design. A three-step permeate pressure that approximates the optimum reduces both the entropy production and the compressor power, when the permeate gas is re-compressed.

Keywords: optimal control theory, membrane, gas separation, lost work

1. Introduction

Semipermeable membranes have many applications in gas separation, and they have rapidly become a competitive solution since their commercial production started [1]. One of the most important fields of application is separation of carbon dioxide (CO_2) from natural gas [1]. Carbon dioxide is present in the natural gas at the extraction. Its removal from natural gas is mandatory to meet pipeline specifications, since it lowers the heat of combustion, it might cause corrosion problems, and it freezes at relatively high temperatures [2]. Removal of CO_2 with alkanolamine solutions has been dominating the field for years, as it allows an almost negligible loss of hydrocarbons [3]. However, under many circumstances, membrane systems are nowadays a competitive alternative, especially for high concentration of CO_2 in the natural gas [4].

*Corresponding author. Tel.: +47-73594183
Email address: elisa.magnanelli@ntnu.no (Elisa Magnanelli)

This is the accepted version of an article published in Computers and Chemical Engineering
DOI: 10.1016/j.compchemeng.2018.06.002

Despite the many advantages of membrane systems, such as small footprint and ease of operation [1], the main drawback remains the relatively low selectivity, which makes the costs due to methane losses high. In order to mitigate this drawback, the permeate gas is usually re-compressed to undergo further separation stages [5]. However, this solution brings additional costs due to investments in additional compressors and to the power necessary for their operation. These costs often become the largest costs in membrane separation systems [6]. For this reason, many studies have been done to minimize the costs of such systems, while maintaining competitive performances [7–14]. Most approaches to the optimization problem have discussed the selection of the optimal stage configurations with permeate and/or retentate recycling, which minimize the costs connected with surface area, methane losses, and compression power [7, 8, 12, 15]. Two- or three-stage configurations are usually necessary to satisfy the requirements on separation. The desired methane losses also play a fundamental role in determining the minimum required membrane area [13]. Another approach considers the use of membranes with different selectivies in different stages [5, 10, 16].

A limitation of optimization results based on cost analysis is that they are affected by fluctuations in natural gas and energy prices. Moreover, the implementation of carbon taxes in many parts of the world can further influence the results [17].

With attention to energy saving, we suggest the use of a different approach, namely the one that minimizes the losses of useful work. Even though membrane processes do not require direct input of heat or power, work is lost as part of the pressurized gas permeates through the membrane and expands to a lower pressure. In most applications, the permeate needs to be re-compressed, either to undergo the next separation stage or to be re-injected into a reservoir. To decrease the work that is lost during the permeation process means to reduce the power necessary to compress the permeate gas.

The lost work in a process can be evaluated through its total entropy production. Indeed, the lost work, W_{lost}, is uniquely related to the entropy that is produced during the process, Σ_{irr}, by the Gouy-Stodola theorem [18]:

$$W_{lost} = T_0 \Sigma_{irr} \tag{1}$$

The use of nonequilibrium thermodynamics allows us not only to assess the total entropy production, but also to exactly determine where in the system entropy is produced and in which amounts [19]. This knowledge enables us to individuate the parts of the system where the largest part of useful work is lost, and where the efforts should be focused in order to improve the system. By combining the nonequilibrium thermodynamic framework and an optimization procedure, it is possible to individuate how the thermodynamic variables should be operated in order to increase the system efficiency. To minimize the entropy production in a system corresponds to finding the system operation where the lost work is minimum. By imposing constraints on the inputs and on the separation of the process, one can guarantee that the economic benefits of the process are maintained. Entropy production minimization has been used not only in connection with nonequilibrium thermodynamics, but also in combination with finite time thermodynamics, resulting in studies of many different applications, such as heat exchangers [20–24], chemical reactors [25–27], and distillation columns [28–34].

This is the accepted version of an article published in Computers and Chemical Engineering
DOI: 10.1016/j.compchemeng.2018.06.002

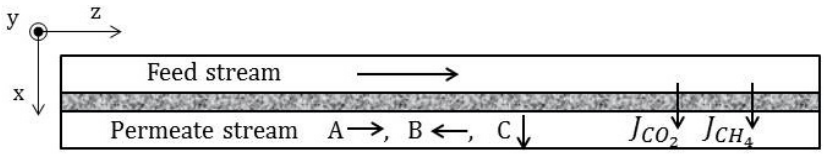

Figure 1: A schematic representation of the system. The feed stream flows in the z-direction parallel to the membrane, which separate the feed and permeate streams. The component molar fluxes, J_{CO_2} and J_{CH_4}, cross the membrane perpendicularly to it (x-direction). The permeate can flow in the same direction as the feed stream (A), in opposite direction (B), or perpendicularly to it (C).

The main purpose of this work is to investigate the possibility of reducing the entropy production in membrane systems, and thus their electric power requirements, by properly controlling the permeate pressure. The aim is to obtain a deeper insight into the process and to develop guidelines on how thermodynamic variables such as pressure should be controlled to enable a reduction of lost work. The results obtained with optimal control theory are used as ideal limits to guide practical design.
In order to isolate the effect of optimal control of the permeate pressure, non-isothermal effects due to gas expansion and compression are neglected in the present work. In actual membrane units, heating is also necessary to compensate for the temperature drop that takes place when the high-pressure natural gas expands through the membrane. Moreover, intercoolers are needed to cool down the gas stream after each compressor. By using the total entropy production as objective function, the optimization procedure can then be easily extended to also take the performance of heaters and coolers into account. Since membrane systems, heat exchangers and compressors require energy inputs that differ in quality, the analysis is not trivial when a first-law parameter such as for instance electric power consumption is used as objective function of the optimization procedure.
After presenting the system in Section 2, we introduce the thermodynamic model and formulate the mathematical optimization problem in Section 3. Details on the solution procedure and relevant data are provided in Section 4, as well as a description of the different cases which are addressed. Results are presented and discussed in Section 5. Conclusions are drawn in Section 6.

2. System

We consider a membrane unit for separation of CO_2 from natural gas. Figure 1 shows a schematic representation of the system. The feed and permeate streams are separated by the membrane. The feed stream flows from left to right, and consists of high pressure natural gas. The permeate side of the membrane is kept at low pressure. Due to the different thermodynamic driving forces and transport coefficients, the two components permeate through the membrane at different rates. When the system is in a stationary state, the fluxes across the membrane are constant in the x-direction.
In order to isolate the effect due to the optimal control of the permeate pressure, we make some simplifying assumptions:

This is the accepted version of an article published in Computers and Chemical Engineering
DOI: 10.1016/j.compchemeng.2018.06.002

– the gas on both sides of the membrane is perfectly mixed in the x- and y-direction (plug flow). The assumption is justified by the fact that the permeation rates and selectivity of commercial membranes are much lower than those for which concentration polarization phenomena occur [35];

– methane and CO_2 are the only two components considered in the mixture. Higher hydrocarbons and water are also normally present in natural gas at the extraction, but their fraction is reduced through cooling and compression ahead of the separation unit [36];

– pressure drops due to viscous flow are neglected, as they are typically small [37]. In a previous work [38], the pressure drop of a similar membrane unit was found to below 0.07 bar. This pressure drop is small in comparison with the pressure drop across the membrane, and it does not influence the thermodynamic properties of the gas significantly. Moreover, since the length of the membrane unit is not a parameter in the optimization procedure, the pressure drop in the different cases will be approximately the same, hence not influencing the results from the optimization procedure;

– diffusive fluxes along the z-direction are neglected, since they are small in comparison to the convective flow;

– the transport coefficients are assumed to be constant;

– the gas is considered to be ideal. This hypothesis has shown to hide a temperature drop along the membrane unit due to the Joule-Thomson effect (circa 15 K temperature difference between inlet and outlet of the feed gas for a similar membrane system [38]). However, the permeabilities of components are to a large extent unaffected by this phenomenon [39, 40];

– no heat is exchanged with the surroundings. This assumption, together with the fact that the gas is considered ideal, results in constant temperature throughout the system.

When optimization is carried out, we assume that we are able to control either the component partial pressures or the total pressure on the permeate side at every position along the z-coordinate. We consider three possible configurations for the permeate side:

A – Co-current: The permeate stream flows parallel to the feed stream, and it has the same flow direction (from left to right in Fig. 1). The left end on the permeate side is a dead-end. This condition is typical of hollow fiber membranes, where a sweep gas is not present.

B – Counter-current: The permeate stream flows parallel to the feed stream, but in the opposite direction (from right to left in Fig. 1). The right end on the permeate side is a dead-end.

C – Cross-flow: The permeate stream flows perpendicular to the feed side (x-direction), and it leaves the unit as it has permeated the membrane.

This is the accepted version of an article published in Computers and Chemical Engineering
DOI: 10.1016/j.compchemeng.2018.06.002

3. Theoretical formulation

In Section 3.1, we present the conservation equations used to describe the system. In Section 3.2, we formulate the entropy production of the system, which represent the objective function of the optimization. Finally, the optimization problems are described in Section 3.3, while Section 3.4 presents the constraint imposed on the separation target of the system.

3.1. Conservation equations

The thermodynamic driving forces between feed and permeate side cause permeation of the two components from one side to the other. On the feed side, the molar balance of component i for a cross section of the system on the xy-plane is [41]:

$$\frac{dF_i}{dz} = -WJ_i \tag{2}$$

where F_i is the molar flow rate of the i component on the feed side, W is the width of the membrane (in the y-direction), and J_i is the flux of component i across the membrane. Here, $i = \{CO_2, CH_4\}$. Each flow rate can be written as:

$$F_i = x_i F \tag{3}$$

where F is the total molar flow rate, x_i is the mole fraction of the component i. The sum of the two flow rates gives the total molar flow rate, thus:

$$\frac{dF}{dz} = \frac{d\left(F_{CO_2} + F_{CH_4}\right)}{dz} = -W\sum_i J_i = -WJ \tag{4}$$

where J is the total molar flux across the membrane.

All the thermodynamic variables introduced above refer to the feed side. We indicate the corresponding variables on the permeate side with a similar notation and the addition of the superscript p.

In the co-current case (configuration A), the left extremity of the permeate side ($z = 0$) is a dead-end, thus the molar flow at this location is zero. Since the gas flowing on the permeate side is the result of the feed gas that has permeated through the membrane, the component molar flows on the permeate side, F_i^p, can be described by the algebraic equation [41]:

$$F_i^p = F_i^{in} - F_i \tag{5}$$

where the superscript *in* indicates the variable at the feed inlet ($z = 0$).

Similarly, when the permeate flow is counter-current (configuration B), the mole balance is [41]:

$$F_i^p = F_i^{out} - F_i \tag{6}$$

where the superscript *out* indicates the variable at the feed outlet ($z = L$, where L is the length of the membrane unit). In both co-current and counter-current configuration, the

This is the accepted version of an article published in Computers and Chemical Engineering
DOI: 10.1016/j.compchemeng.2018.06.002

component mole fraction on the permeate side can be calculated as the ratio between the component flow rate and the total flow rate:

$$x_i^p = \frac{F_i^p}{F^p} \tag{7}$$

However, at the permeate inlet of both cases, x_i^p cannot be calculated according to Eq. 7, since the term at the denominator is zero. At this location, the mole fraction of CO_2 and methane is determined by their permeating fluxes, and can be calculated according to the relation:

$$x_i^{p,in} = \frac{J_i}{J} \tag{8}$$

The condition described by Eq. 8, applies at $z = 0$ for the co-current case, and at $z = L$ for the counter-current case.

When the cross-flow is considered (configuration C), the gas that permeates from the feed side to the permeate side leaves the membrane unit immediately, and the component mole fractions on the permeate side are given by Eq. 8 at all positions along the membrane.

Flux-force relations from nonequilibrium thermodynamics [42] can be used to calculate the fluxes across the membrane:

$$J_i = L_i X_i = -L_i \Delta \frac{\mu_i}{T} \tag{9}$$

where X_i is the thermodynamic driving force, μ_i is the component chemical potential, L_i is the component mass transport coefficient, and T is the temperature. Here, Δ indicates the difference between permeate and feed side. Since we consider the gas to be ideal, the chemical potential of a component in the gas phase can be written as:

$$\mu_i = \mu_{0,i} + RT \ln \frac{x_i p}{p_0} \tag{10}$$

where $\mu_{0,i}$ is the component standard chemical potential, R is the universal gas constant, p is the total pressure, and p_0 is the standard state pressure. Introducing Eq. 10 into Eq. 9, we get:

$$J_i = -RL_i \ln \frac{p_i^p}{x_i p} = -RL_i \ln \frac{x_i^p p^p}{x_i p} \tag{11}$$

The component molar fluxes can be calculated from the permeabilities of the membrane material to the two gases, P_i, which is defined according to [43]:

$$J_i = -P_i \frac{p_i^p - p_i}{\delta} \tag{12}$$

where δ is the thickness of the membrane. Comparing Eq. 12 with Eq. 11, we get:

$$L_i = \frac{P_i}{\delta R} \frac{p_i^p - p_i}{\ln\left(p_i^p / p_i\right)} \tag{13}$$

Permeabilities can be found in literature for specific feed and permeate pressures, temperatures, and compositions [44]. The transport coefficients are determined according to Eq. 13 for the relative specific conditions.

This is the accepted version of an article published in Computers and Chemical Engineering
DOI: 10.1016/j.compchemeng.2018.06.002

3.2. Entropy production

The objective function of the optimization problem is the total entropy production of the system, Σ_{irr}. According to nonequilibrium thermodynamics [42], the entropy production of a homogeneous phase can be written as the product sum of all fluxes, J_i, and their conjugate forces, X_i. The entropy production is:

$$\sigma = W \sum_i J_i X_i = W \left(J_{CO_2} X_{CO_2} + J_{CH_4} X_{CH_4} \right) \tag{14}$$

By introducing the flux-force relations given by Eq. 9 into Eq. 14, we obtain the entropy production as a function of the driving forces only:

$$\begin{aligned} \sigma &= W \left(L_{CO_2} X_{CO_2}^2 + L_{CH_4} X_{CH_4}^2 \right) \\ &= W \left(L_{CO_2} \left(-\Delta \frac{\mu_{CO_2}}{T} \right)^2 + L_{CH_4} \left(-\Delta \frac{\mu_{CH_4}}{T} \right)^2 \right) \end{aligned} \tag{15}$$

The total entropy production is found by integrating the entropy production over the total length of the membrane unit:

$$\Sigma_{irr} = \int_0^L \sigma dz \tag{16}$$

By introducing Eqs. 11 and 15 into Eq. 16, we get:

$$\begin{aligned} \Sigma_{irr} &= W \int_0^L L_{CO_2} \left(-R \ln \frac{p_{CO_2}^p}{x_{CO_2} p} \right)^2 + L_{CH_4} \left(-R \ln \frac{p_{CH_4}^p}{x_{CH_4} p} \right)^2 dz \\ &= \Sigma_{irr,CO_2} + \Sigma_{irr,CH_4} \end{aligned} \tag{17}$$

The total entropy production has two contributions. The first one is due to transfer of CO_2, Σ_{irr,CO_2}, while the second one is due to methane transfer, Σ_{irr,CH_4}. An alternative derivation of the total entropy production, which uses the entropy balance equation as starting point, is provided in Appendix A.

3.3. The optimization problem

The aim of the work is to minimize the total entropy production of the system with given constrains, taking advantage of optimal control theory. Eight variables are necessary to completely describe the system at any point along the z-coordinate: CO_2 and CH_4 molar flow rates, temperature and pressure, on both feed and permeate side.In the reference case, where no control is operated, the behavior of the height variables is dictated either by the mass balances (that determine the components flow rates) or by specifications (constant pressure and temperature). The reference system has, thus, zero degrees of freedom.

According to optimal control theory, the variables of relevance in a controlled system can be classified in independent state variables and in control variables [45]. Further details and an introduction to optimal control theory can be found in Refs. [45, 46].

The state variables are the variables in the system that are governed by differential equations. According to the formulation reported in Section 3.1, F_{CO_2} and F_{CH_4} are the

This is the accepted version of an article published in Computers and Chemical Engineering
DOI: 10.1016/j.compchemeng.2018.06.002

state variables. Since we assume that no gas is fed on the permeate side, the values that the component flow rates can attain are constrained by the relations:

$$F_i^{in} - F_i \geq 0 \tag{18}$$

Thus, the state variables are subject to constraints. In order to ensure that the state variable constraints are not violated during the optimization procedure, it is necessary to define a new variable F_{SC}, whose spatial derivative is defined as [46]:

$$\frac{dF_{SC}}{dz} = \xi_{CO_2}\left(F_{CO_2}^{in} - F_{CO_2}\right) + \xi_{CH_4}\left(F_{CH_4}^{in} - F_{CH_4}\right) \tag{19}$$

where ξ_{CO_2} and ξ_{CH_4} are step functions defined as:

$$\xi_i = \begin{cases} 0, & \text{for } F_i^{in} - F_i \geq 0 \\ 1, & \text{for } F_i^{in} - F_i < 0 \end{cases}$$

Equation 19 needs to be equal to 0 in order for all state constraints to be satisfied. By imposing the two boundary conditions $F_{SC}(0) = 0$ and $F_{SC}(L) = 0$, we ensure that the state constraints are fulfilled everywhere along the spatial coordinate [46].
The control variables are those variables used to control the system. The permeate partial pressures are used as controls when we control two variables, while the permeate total pressure is used when only one variable is controlled.
According to optimal control theory, the conditions for a minimum in the objective function can be derived from the Hamiltonian of the problem [46]:

$$\begin{aligned} H \quad = \quad & \sigma + \lambda_{CO_2}\left(-WJ_{CO_2}\right) + \lambda_{CH_4}\left(-WJ_{CH_4}\right) \\ & + \lambda_{SC}\left(\xi_{CO_2}\left(F_{CO_2}^{in} - F_{CO_2}\right) + \xi_{CH_4}\left(F_{CH_4}^{in} - F_{CH_4}\right)\right) \end{aligned} \tag{20}$$

The Hamiltonian has two contributions. The first contribution is given by the integrand in the total entropy production equation (i.e. the entropy production). The second contribution is constituted by the product of the multipliers' functions, λ_i, and the right-hand side of the state variable governing equations [46] (including the fictitious state variable defined by Eq. 19).
The necessary conditions for a minimum and for the fulfillment of the state constraints are represented by 2 differential equations for each state variable (including the fictitious one), and by 1 algebraic equation for each control variable [45]. Thus, we have 6

This is the accepted version of an article published in Computers and Chemical Engineering
DOI: 10.1016/j.compchemeng.2018.06.002

differential necessary conditions for the problem:

$$\frac{dF_{CO_2}}{dz} = \frac{\partial H}{\partial \lambda_{CO_2}} \tag{21}$$

$$\frac{dF_{CH_4}}{dz} = \frac{\partial H}{\partial \lambda_{CH_4}} \tag{22}$$

$$\frac{dF_{SC}}{dz} = \frac{\partial H}{\partial \lambda_{SC}} \tag{23}$$

$$\frac{d\lambda_{CO_2}}{dz} = -\frac{\partial H}{\partial F_{CO_2}} \tag{24}$$

$$\frac{d\lambda_{CH_4}}{dz} = -\frac{\partial H}{\partial F_{CH_4}} \tag{25}$$

$$\frac{d\lambda_{SC}}{dz} = -\frac{\partial H}{\partial F_{SC}} \tag{26}$$

The left sides of Eqs. 21-23 equal the conservation equations (Eqs. 2 and 19). Equations 24-26 describe the evolution in space of the Lagrangian multipliers. Since the Hamiltonian is not a direct function of F_{SC}, Eq. 26 equals zero, and λ_{SC} is constant. By expressing the Hamiltonian as a function of the state variables, and carrying out the partial differentiations, Eqs. 24-25 can be reformulated as:

$$\begin{aligned}\frac{d\lambda_{CO_2}}{dz} = {} & WRL_{CO_2}(2X_{CO_2} - \lambda_{CO_2})\left(\frac{1}{x^p_{CO_2}}\frac{\partial x^p_{CO_2}}{\partial F_{CO_2}} - \frac{x_{CH_4}}{F_{CO_2}}\right) \\ & + WRL_{CH_4}(2X_{CH_4} - \lambda_{CH_4})\left(\frac{1}{x^p_{CH_4}}\frac{\partial x^p_{CH_4}}{\partial F_{CO_2}} + \frac{x_{CH_4}}{F_{CH_4}}\right) \\ & + \lambda_{SC}\xi_{CO_2}\end{aligned} \tag{27}$$

$$\begin{aligned}\frac{d\lambda_{CH_4}}{dz} = {} & WRL_{CO_2}(2X_{CO_2} - \lambda_{CO_2})\left(\frac{1}{x^p_{CO_2}}\frac{\partial x^p_{CO_2}}{\partial F_{CH_4}} + \frac{x_{CO_2}}{F_{CO_2}}\right) \\ & + WRL_{CH_4}(2X_{CH_4} - \lambda_{CH_4})\left(\frac{1}{x^p_{CH_4}}\frac{\partial x^p_{CH_4}}{\partial F_{CH_4}} - \frac{x_{CO_2}}{F_{CH_4}}\right) \\ & + \lambda_{SC}\xi_{CH_4}\end{aligned} \tag{28}$$

The partial derivatives of the permeate mole fraction are derived in Appendix B.1. Their expressions are different for different permeate configurations.

3.3.1. Optimal case with 2 control variables

Since the reference system has zero degrees of freedom, we first need to disregard some of the specifications on the system variables, in order to gain sufficient freedom to control the system. In this case, we eliminate the specification of constant pressure on the permeate side, as well as we neglect one of the component balances on the permeate side. This allows the system to gain two degrees of freedom that can be used to control the system.

This is the accepted version of an article published in Computers and Chemical Engineering
DOI: 10.1016/j.compchemeng.2018.06.002

Several meaningful choices of control variables can be made. We choose to use the permeate partial pressures as control variables, and we assume to be able to control them completely. Since we control these variables at any position along the membrane, the permeate mole fractions are determined everywhere according to:

$$x_i^p = \frac{p_i^p}{p^p} \tag{29}$$

Since the permeate mole fraction is a function of the permeate partial pressures only, the partial derivatives of x_i^p in Eqs. 27-28 are zero. In this case, the Hamiltonian is not explicitly dependent on the spatial coordinate (i.e. it is autonomous), and therefore it is constant in space [45].
When two variables can be controlled, we also have two algebraic equations as necessary conditions for a minimum:

$$\frac{\partial H}{\partial p_{CO_2}^p} = 0 \tag{30}$$

$$\frac{\partial H}{\partial p_{CH_4}^p} = 0 \tag{31}$$

When the number of control variables equals, as in this case, the number of independent state variables, we have enough control to be able to control all driving forces independently [25]. Thus, we can use the driving forces instead of the permeate partial pressures as the control variables. Equations 30 and 31 can then be replaced by:

$$\frac{\partial H}{\partial X_{CO_2}} = WL_{CO_2}\left(2X_{CO_2} - \lambda_{CO_2}\right) = 0 \tag{32}$$

$$\frac{\partial H}{\partial X_{CH_4}} = WL_{CH_4}\left(2X_{CH_4} - \lambda_{CH_4}\right) = 0 \tag{33}$$

Solving the two equations for λ_{CO_2} and λ_{CH_4} and substituting into Eq. 20, we get:

$$H = -\sigma + \lambda_{SC}\left(\xi_{CO_2}\left(F_{CO_2}^{in} - F_{CO_2}\right) + \xi_{CH_4}\left(F_{CH_4}^{in} - F_{CH_4}\right)\right) \tag{34}$$

As mentioned above, the Hamiltonian is constant along the spatial coordinate, while the last term in Eq. 34 is 0 for any admissible solutions. The entropy production is, thus, constant across the system, when the system is optimally controlled.
Equations 32-33 can be reformulated to obtain an explicit expression for the two control variables:

$$p_{CO_2}^p = x_{CO_2} p \cdot \exp\left(-\frac{\lambda_{CO_2}}{2R}\right) \tag{35}$$

$$p_{CH_4}^p = x_{CH_4} p \cdot \exp\left(-\frac{\lambda_{CH_4}}{2R}\right) \tag{36}$$

Substituting Eqs. 32 and 33 into Eqs. 27-28, and considering that ξ_i are equal to 0 for a feasible solution, we find that the spatial derivatives of the multipliers are zero, and therefore λ_{CO_2} and λ_{CH_4} are constant.

This is the accepted version of an article published in Computers and Chemical Engineering
DOI: 10.1016/j.compchemeng.2018.06.002

3.3.2. Optimal case with 1 control variable

When one variable is controlled, one specification on the system variables needs to be eliminated. The most relevant single control variable in our case is the total permeate pressure, p^p. Thus, the specification of constant permeate pressure is disregarded, and the system gains one degree of freedom that can be used to control the system.
The minimization problem is characterized by the same 6 differential necessary conditions presented above (Eqs. 21-26). However, the optimal problem has now one algebraic necessary condition only. For the co-current and the counter-current configuration, the condition is:

$$\begin{aligned}\frac{\partial H}{\partial p^p} &= -\frac{WRL_{CO_2}}{p^p}\left(2X_{CO_2}-\lambda_{CO_2}\right)\\ &\quad -\frac{WRL_{CH_4}}{p^p}\left(2X_{CH_4}-\lambda_{CH_4}\right)=0\end{aligned} \tag{37}$$

By expressing the driving forces as functions of the permeate pressure, Eq. 37 can be reformulated to give an explicit expression for p^p:

$$\begin{aligned}p^p &= p\left(\frac{x_{CO_2}}{x^p_{CO_2}}\right)^{\frac{L_{CO_2}}{L_{CO_2}+L_{CH_4}}}\left(\frac{x_{CH_4}}{x^p_{CH_4}}\right)^{\frac{L_{CH_4}}{L_{CO_2}+L_{CH_4}}}\\ &\quad \cdot\exp\left(-\frac{\lambda_{CO_2}L_{CO_2}+\lambda_{CH_4}L_{CH_4}}{2R\left(L_{CO_2}+L_{CH_4}\right)}\right)\end{aligned} \tag{38}$$

In the cross-current case as well as at the permeate inlet in the co-current and counter-current configuration, the composition on the permeate side depends on p^p through Eq. 8. Thus, the necessary condition has two additional terms:

$$\begin{aligned}\frac{\partial H}{\partial p^p} &= -WRL_{CO_2}\left(\frac{1}{p^p}+\frac{1}{x^p_{CO_2}}\frac{\partial x^p_{CO_2}}{\partial p^p}\right)\left(2X_{CO_2}-\lambda_{CO_2}\right)\\ &\quad -WRL_{CH_4}\left(\frac{1}{p^p}+\frac{1}{x^p_{CH_4}}\frac{\partial x^p_{CH_4}}{\partial p^p}\right)\left(2X_{CH_4}-\lambda_{CH_4}\right)=0\end{aligned} \tag{39}$$

Since it is not possible to find an analytical expression for p^p from Eq. 39, the permeate pressure is computed numerically. The partial derivatives of the permeate composition with respect to the permeate partial pressure are derived in Appendix B.2.

3.4. Constraint

In order to have a meaningful optimization, we need to impose at least one constraint on the separation of the membrane unit. Pipeline specifications impose natural gas CO_2 fraction lower than 2%. We therefore require the CO_2 mole fraction in the retentate gas leaving the membrane unit to satisfy the pipeline requirements:

$$x^{out}_{CO_2}=0.02,\quad z=L \tag{40}$$

This constraint is applied to both optimization problems.

This is the accepted version of an article published in Computers and Chemical Engineering
DOI: 10.1016/j.compchemeng.2018.06.002

4. Solution procedure

Before solving the optimization problem, we establish the entropy production of a reference process where no control is operated on the system. Two differential equations describe the reference process (Eq. 2 for CO_2 and methane). We consider three different flow configurations on the permeate side (Case A, Case B, and Case C). The nature of the mathematical problem is different in different configurations. Case A and Case C are initial value problems, while the counter-current case (Case B) is a boundary value problem. We use the Matlab "ode15s" multistep solver to integrate the initial value problems, while we deal with the boundary value problem using the Matlab "bvp4c" solver, which exploits a collocation method. Constant flow profiles equal to the inlet values, $F^{in}_{CO_2}$ and $F^{in}_{CH_4}$, are provided as initial guesses (derived from the data reported in Table 1).

The case with the lowest entropy production is chosen to be the reference membrane process for comparison with the optimal results. The optimization problem is characterized by 3 additional differential equations (5 differential equations in total) and one unknown parameter (λ_{SC}), that describe the evolution in space of the Lagrangian multipliers and of the additional state variable (Eqs. 23-26). Six boundary conditions are thus needed to solve the problem. The 2 first boundary conditions are the same for reference and optimal case (i.e. $F_{CO_2}(z=0) = F^{in}_{CO_2}$ and $F_{CH_4}(z=0) = F^{in}_{CH_4}$). Additional boundary conditions are given by the constraint on the duty of the system (Eq. 40), by the 2 boundary constraints imposed on the additional state variable ($F_{SC}(z=0) = 0$ and $F_{SC}(z=L) = 0$). Finally, the last boundary condition concerns the Lagrange multipliers. It is derived from the constraints on the state variables at the final state as [46]:

$$0.02\lambda_{CO_2} + 0.98\lambda_{CH_4} = 0, \quad z = L \tag{41}$$

This condition is usually called terminal condition.

Since some boundary conditions are specified at the inlet ($z = 0$) , while others at the outlet ($z = L$), the optimization problems are boundary value problems. Therefore, we use the Matlab "bvp4c" solver to solve them. For the solution of the first optimization problem, the feed flow profiles obtained for the reference case and two constant profiles (we arbitrary use the constant value 1) are used as initial guesses for component flow rates and Lagrangian multipliers. The optimal results obtained from the first optimization problem are used as initial guesses for the solution of the second one.

4.1. Input data

Calculations are performed at a set of operating conditions typical of natural gas purification membrane units (Table 1). The pressure ratio between feed and permeate side is very large, since it represents the driving force responsible for the component permeation though the membrane. In the calculations of the reference cases, the pressure ratio equals 50, which is a normal value for such applications. Since the pressure drops due to the viscous flow are neglected, the total pressure on the feed side is constant. The same applies to the permeate pressure in the reference case. A summary of the most important membrane parameters is reported in Table 2. The data for CO_2 and methane permeability in cellulose acetate are taken from Ref. [44]. Tables 1 and 2 contain the data used to derive the boundary conditions for the problem.

This is the accepted version of an article published in Computers and Chemical Engineering
DOI: 10.1016/j.compchemeng.2018.06.002

Table 1: Operating conditions for the reference membrane process [47]. In the reference process, the pressure on both sides are constant along the z-direction. The same constant temperature is considered at the two sides of the membrane. Since the inlet end on the permeate side is a dead-end (configuration A and B), the permeate flow at the inlet is zero. The composition at the inlet of the permeate side is given by the ratio of the permeating fluxes at this location (Eq. 8).

	Value	Units
T	308	K
p	$50{\cdot}10^5$	Pa
p^p	$1{\cdot}10^5$	Pa
F^{in}	0.195	$\text{mol}{\cdot}\text{s}^{-1}$
$F^{p,in}$	0	$\text{mol}{\cdot}\text{s}^{-1}$
$x^{in}_{CO_2}$	0.3	-

Table 2: Parameters of the membrane unit. The transport coefficients, L_{CO_2} and L_{CH_4}, have been calculated from the other membrane parameters according to Eq. 13.

	Value	Units
δ	1	μm
W	1	m
P_{CO_2}	$1.5{\cdot}10^{-15}$	$\text{mol}{\cdot}\text{m}^{-1}{\cdot}\text{s}^{-1}{\cdot}\text{Pa}^{-1}$
P_{CH_4}	$5.8{\cdot}10^{-17}$	$\text{mol}{\cdot}\text{m}^{-1}{\cdot}\text{s}^{-1}{\cdot}\text{Pa}^{-1}$
L_{CO_2}	$7.9{\cdot}10^{-5}$	$\text{mol}^2{\cdot}\text{K}\cdot\text{m}^{-2}{\cdot}\text{s}^{-1}{\cdot}\text{J}^{-1}$
L_{CH_4}	$5.7{\cdot}10^{-6}$	$\text{mol}^2{\cdot}\text{K}\cdot\text{m}^{-2}{\cdot}\text{s}^{-1}{\cdot}\text{J}^{-1}$

4.2. Investigated cases

In this work, we progressively evaluate and compare different cases. For sake of clarity, from now on, they are named as follows:

Ref.: In the reference case no optimal control takes place. Three different flow configurations are compared, according to the description in Section 2 (Ref. A, Ref. B, and Ref. C). In every configuration, the length of the membrane unit is such to give $x^{out}_{CO_2} = 0.02$. The length of the best performing configuration (i.e. the length of the shortest unit) will be taken as the unit length in all optimization problems.

Opt. 2cv: The process is optimally controlled by control of the permeate partial pressures. The corresponding mathematical problem was described in Section 3.3.1. Since the number of control variables is sufficient to control the two driving forces independently, the permeate configuration does not influence the results.

Opt. 1cv: The process is optimally controlled by control of the permeate total pressure only. The corresponding mathematical problem was presented in Section 3.3.2. The optimization problem is solved for different permeate configurations (Opt. 1cvA, Opt. 1cvB, and Opt. 1cvC).

This is the accepted version of an article published in Computers and Chemical Engineering
DOI: 10.1016/j.compchemeng.2018.06.002

Table 3: Performances of the membrane reference cases, for co-current case (Ref. A), counter-current case (Ref. B), and cross-flow (Ref. C). The lengths of the membrane units are such to give $x^{out}_{CO_2} = 0.02$. $W_{recompr}$ indicate the compression power necessary to re-compress the permeate gas to 50 bar.

	Ref. A	Ref. B	Ref. C	Units
$x^{out}_{CO_2}$	0.02	0.02	0.02	-
L	46.4	41.6	42.8	m
$F^{p,out}_{CH_4}$	$1.26 \cdot 10^{-2}$	$1.05 \cdot 10^{-2}$	$1.12 \cdot 10^{-2}$	mol·s^{-1}
Σ_{irr}	1.618	1.517	1.547	J·K^{-1}·s^{-1}
Σ_{irr,CO_2}	1.021	1.056	1.035	J·K^{-1}·s^{-1}
Σ_{irr,CH_4}	0.597	0.461	0.512	J·K^{-1}·s^{-1}
W_{compr}	688	666	674	W

5. Results

5.1. Reference cases

Table 3 reports the results obtained for the three different permeate flow configurations, when no optimal control is operated. The membrane unit length in the different configurations are determined so that they give the same CO_2 mole fraction in the retentate ($x^{out}_{CO_2} = 0.02$). Ref. A is the case that requires the longest membrane unit (circa 10% longer than in Ref. B, and 8% longer than in Ref. C).

The counter-current configuration is confirmed to be the most economically advantageous, since it allows to save part of the investment costs due to the smaller membrane surface, and it gives smaller methane losses, $F^{p,out}_{CH_4}$. However, the counter-current configuration is the most convenient also from a thermodynamic perspective. Indeed, its total entropy production and, therefore, its lost work are lower than in the other cases (circa 6% and 2% lower than Ref. A and Ref. C respectively). When the permeate gas needs to be re-compressed (either to be re-injected into the reservoir or to undergo a new separation stage), the counter-current configuration requires less compression power than the other configurations (Eq. D.1). In the case that permeate gas is re-compressed to the original pressure of 50 bar, the counter-current configuration requires 3.2% less power than the co-current case.

Figure 2 shows the entropy production obtained with Ref. A (thick solid line), Ref. B (thick dashed line), and Ref. C (thin solid line). Since the length of the membrane unit is different for the different configurations, the entropy production is reported as a function of the normalized z-coordinate (i.e. the coordinate value divided by the length of membrane unit). The shape of the entropy production profiles does not differ much between the cases, and the difference in the total entropy production of the process is mainly due to the integration over a different length.

None of the reference cases is optimally controlled to yield minimum entropy production. Since the counter-current case produces the least amount of entropy, we choose Ref. B to be the reference case for further calculations. In the remaining part of Section 5, we will refer to it as Ref., and we will use $L = 41.6$ m from the counter-current configuration as length of the membrane unit during optimization.

This is the accepted version of an article published in Computers and Chemical Engineering
DOI: 10.1016/j.compchemeng.2018.06.002

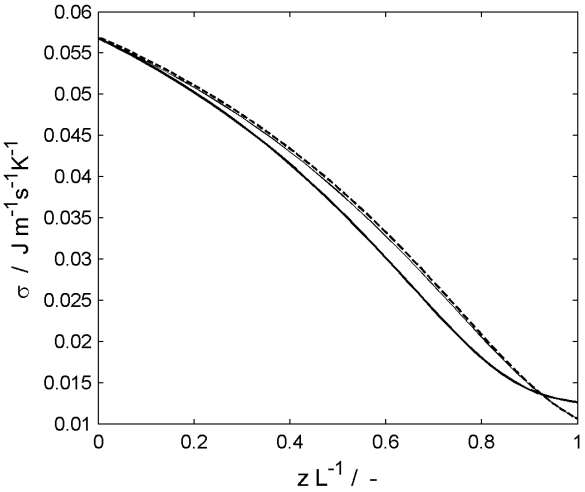

Figure 2: Local entropy production, in the Ref. A (thick solid line), Ref. B (thick dashed line), and Ref. C (thin solid line). The thick dashed line and the thin solid line are almost superimposed at this scale.

In order to check the consistency of the thermodynamic framework presented in Section 3, the total entropy production has been calculated for all investigated cases according to both Eq. 17 and Eq. A.1. The relative error between the results given by the two equations are order of the numerical accuracy of the calculations (10^{-6}).

5.2. Comparison between analytical and numerical optimization

The conditions for optimality presented in Section 3.3 define only the necessary conditions for a minimum. Therefore, in order to evaluate whether the identified results correspond to the global minimum, the optimal results presented in Sections 5.3-5.4 were compared with those obtained by solving the optimization problem numerically. Details on the numerical solution of the problem are presented in Appendix C. However, a numerical optimization does also not guarantee that we find the global minimum. Thus, the numerical optimization procedure was carried out for different random initial profiles. If another minimum existed, it would have most likely been found by following this procedure. Since the results obtained with the analytical optimization and those obtained by numerical optimizations carried out with different random starting points coincided, we can assume that the minima that have been identified are global ones.

The relative error between the profiles given by the analytical and numerical optimization procedures is order of the numerical accuracy of calculations (relative accuracy of 10^{-6}). Right at the boundaries, the relative error is larger (10^{-3}). This is due to the fact that the spatial derivative approximation used for the numerical optimization has lower accuracy at the boundaries. Even though analytical and numerical methods give the same solution, the analytical one leads to more accurate results in a shorter time.

This is the accepted version of an article published in Computers and Chemical Engineering
DOI: 10.1016/j.compchemeng.2018.06.002

Table 4: Total entropy production of the membrane unit in the reference case (Ref.) and in the optimal case where 2 control variables are available (Opt. 2cv). L = 41.6 m is used as length of the membrane unit.

	Ref.	Opt. 2cv	Units
Σ_{irr}	1.517	0.945	$J{\cdot}K^{-1}{\cdot}s^{-1}$
Σ_{irr,CO_2}	1.056	0.945	$J{\cdot}K^{-1}{\cdot}s^{-1}$
Σ_{irr,CH_4}	0.461	0	$J{\cdot}K^{-1}{\cdot}s^{-1}$

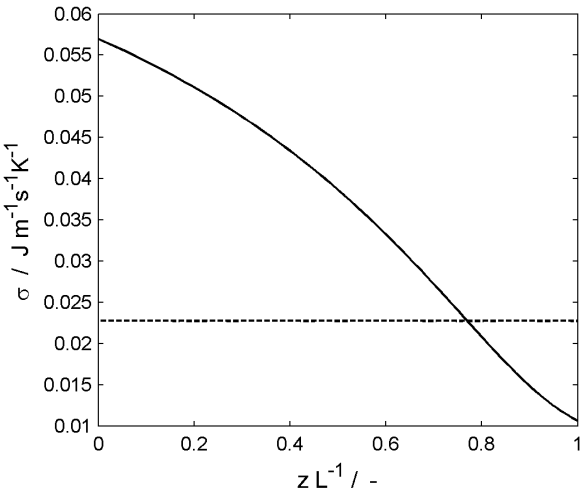

Figure 3: Entropy production for the reference case (solid line) and for Opt. 2cv (dashed line).

Moreover, the mathematical derivation of the analytical optimization problem enables us to get information on the nature of the solution (Section 3.3.1).
Thanks to optimal control theory, the system of differential equations (Eqs. 23-26) can be solved robustly and to a high accuracy for a wide range of operating conditions. The advantage of using optimal control theory instead of direct gradient- or trust-region based optimization methods, is that one has excellent control of the accuracy of the optimal configuration through the error-control of the boundary value solver.

5.3. Optimal case with 2 control variables

In this section, we assume to have full control on the permeate partial pressures. The results obtained with optimal control are compared with those of the reference case (Ref.). Since we control the permeate partial pressure at any position, the results are independent of the permeate flow configuration. Table 4 shows that optimal control of the permeate partial pressures allows for a significant reduction in the total entropy production (circa 38%). The reduction is mainly due to the fact that the methane permeating flux reduces to zero. Therefore, by controlling both components' partial pressures it is in principle possible to reduce the methane losses to zero.

This is the accepted version of an article published in Computers and Chemical Engineering
DOI: 10.1016/j.compchemeng.2018.06.002

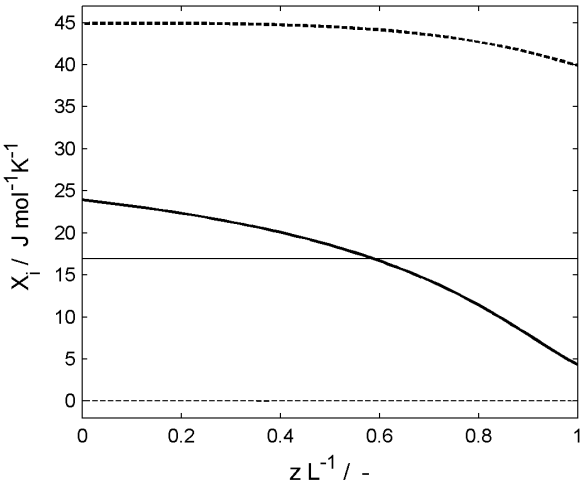

Figure 4: Thermodynamic driving forces across the membrane for CO_2 (solid lines) and methane (dashed lines), for the reference case (thick lines) and for Opt. 2cv (thin lines).

Figure 3 compares the entropy production of the reference case (solid line) with the one of Opt. 2cv (dashed line). The results show that the entropy production is indeed constant when we can control all driving forces independently (dashed line), confirming what was found theoretically in Section 3.3.1.
Figure 4 shows the thermodynamic driving forces across the system for Ref. (thick lines) and for Opt. 2cv (thin lines). In the optimally controlled case, the driving forces for CO_2 and methane transport are both constant. In particular, the driving force to methane transport is everywhere equal to zero.
In practice, the control of both permeate partial pressures is almost impossible. However, this case is interesting from a theoretical point of view. Indeed, the entropy production in the present optimal case represents the lower bound for the production of entropy of a membrane system subject to specific separation constraints and boundary conditions. A real process that takes place in finite time and space produces an inevitable amount of entropy, and, thus, it looses some useful work [48]. The minimum amount of work that is inevitably lost depends on the boundary conditions and constraints assigned to the problem. When constraints and boundary conditions are fixed, the minimum lost work and the minimum entropy production can be calculated by optimizing the system under the assumption that we can control all driving forces.

5.4. Optimal case with 1 control variable

In this section, the performances of the reference case (Ref.) are compared with the optimal case in which we control the total permeate pressure only. Since the driving forces depend on both total pressure and composition of the permeate side, we cannot control the driving forces independently. In this case, the results of the optimization depend on the permeate flow configuration.

This is the accepted version of an article published in Computers and Chemical Engineering
DOI: 10.1016/j.compchemeng.2018.06.002

Table 5: Performances of the membrane unit in the reference case (Ref.) and in the optimal cases where 1 control variable is available (Opt. 1cvA, Opt. 1cvB, and Opt. 1cvC). The reduction in the total entropy production is expressed with respect to the one of the reference case. L = 41.6 m is used as length of the membrane unit.

	Ref.	Opt. 1cvA	Opt. 1cvB	Opt. 1cvC	Units
Σ_{irr}	1.517	1.447	1.420	1.436	$J{\cdot}K^{-1}{\cdot}s^{-1}$
Reduction in Σ_{irr}	–	-4.6	-6.4	-5.4	%
Σ_{irr,CO_2}	1.056	0.957	0.953	0.953	$J{\cdot}K^{-1}{\cdot}s^{-1}$
Σ_{irr,CH_4}	0.461	0.490	0.467	0.483	$J{\cdot}K^{-1}{\cdot}s^{-1}$
$F_{CH_4}^{p,out}$	$1.050 \cdot 10^{-2}$	$1.071 \cdot 10^{-2}$	$1.051 \cdot 10^{-2}$	$1.067 \cdot 10^{-2}$	$mol{\cdot}s^{-1}$

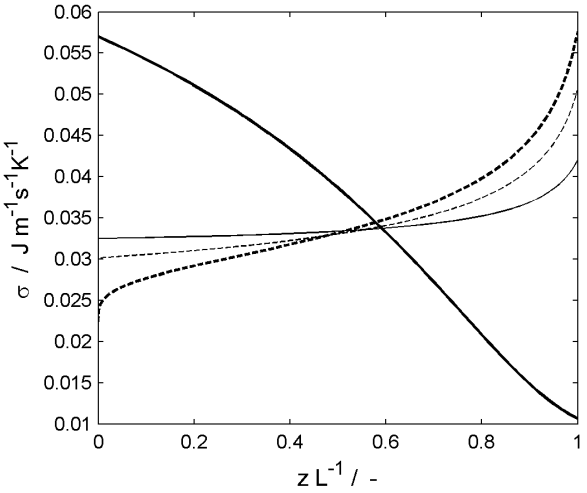

Figure 5: Entropy production for the reference case (thick solid line) and for Opt. 1cvA (thick dashed line), Opt. 1cvB (thin solid line), and Opt. 1cvC (thin dashed line).

Table 5 compares the performance of the reference case with those of the optimal case for different permeate configurations (Opt. 1cvA, Opt. 1cvB, and Opt. 1cvC). The same membrane length is used for all three configurations. With the control of the permeate pressure, the separation constraint can be satisfied with all configurations for the same membrane area. The counter-current configuration (Opt. 1cvB) is nevertheless preferable over the others, as it leads to lower entropy production and to lower methane losses. The entropy production cannot be reduced as much as with control of both permeate partial pressures (maximum reduction of only 6.4% in counter-current configuration). In this case, the reduction in entropy production is only due to lower Σ_{irr,CO_2}, while Σ_{irr,CH_4} is slightly higher than in the reference case (Ref). The fact that the optimization problem only focuses on reducing the contribution due to the CO_2 transport suggests that when there is no independent control on all driving forces, it is particularly beneficial to seek for membrane designs and materials with higher CO_2/methane

This is the accepted version of an article published in Computers and Chemical Engineering
DOI: 10.1016/j.compchemeng.2018.06.002

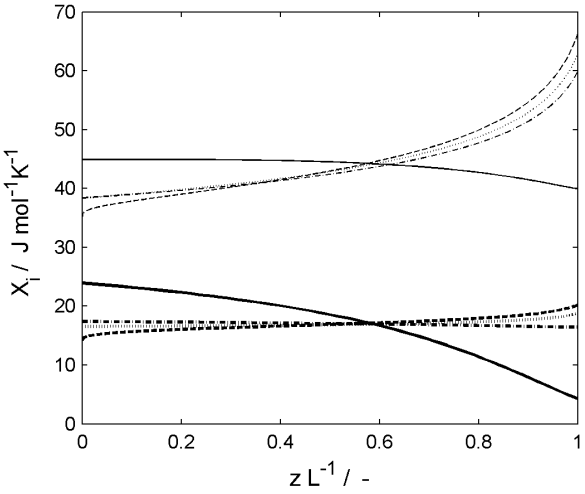

Figure 6: Thermodynamic driving forces across the membrane for CO_2 (thick lines) and methane (thin lines), for the reference case (solid line) and for Opt. 1cvA (dashed line), Opt. 1cvB (dash-dot line), and Opt. 1cvC (dotted line).

Table 6: Total entropy production of the membrane unit for the reference case (Ref.), in the optimal case where 1 control variable is available (Opt. 1cvB), in the case where EoEP is imposed, in the case where EoF_{CO_2} is imposed, and in the case where EoF_{CH_4} is imposed. L = 41.6 m is used as length of the membrane unit.

Σ_{irr} / J·K^{-1}·s^{-1}	Ref	Opt. 1cv	EoEP	EoF_{CO_2}	EoF_{CH_4}
Case A	1.618	1.447	1.463	1.451	1.657
Case B	1.517	1.420	1.421	1.421	1.484
Case C	1.547	1.436	1.442	1.437	1.517

selectivities. With a higher CO_2/methane selectivity, Σ_{irr,CO_2} represents a larger fraction of the total entropy production, and therefore a larger reduction of entropy production is possible, when only the total permeate pressure is controlled.

Figure 5 compares the entropy production for the reference case (thick solid line) with the one obtained in Opt. 1cvA (thick dashed line), Opt. 1cvB (thin solid line), and Opt. 1cvC (thin dashed line). Even if none of the entropy production profiles are constant in this case, σ has a smaller variation when the total entropy production is lower (i.e. Opt. 1cvB).

Figure 6 presents the driving forces in the different cases (solid lines for Ref., dashed lines for Opt. 1cvA, dash-dot lines for Opt. 1cvB, and dotted lines for Opt. 1cvC). As for the entropy production, the forces are not constant in any of the optimally controlled cases. However, the driving force for CO_2 transport (thick lines) is more constant in the optimal cases than in the reference process. On the other hand, the methane driving force (thin lines) varies more in the optimal cases than in the reference case.

In order to further investigate these aspects, we calculated the total entropy production

This is the accepted version of an article published in Computers and Chemical Engineering
DOI: 10.1016/j.compchemeng.2018.06.002

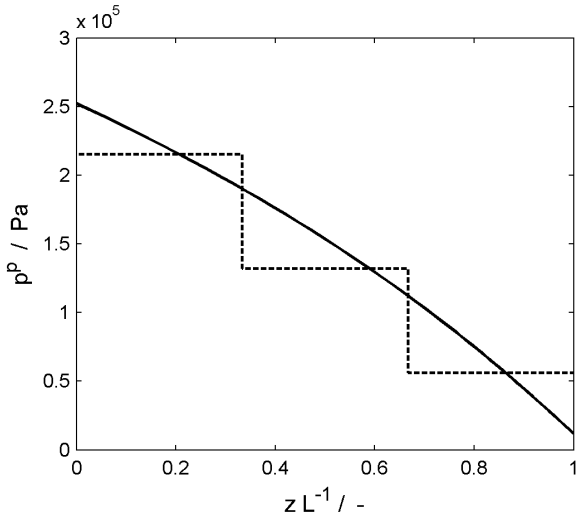

Figure 7: Permeate total pressure for Opt. 1cvB (solid line), and for a three-step approximation of the optimum profile (dashed line).

that results from controlling the permeate pressure to enforce constant driving force either to CO_2 transport (EoF_{CO_2}) or to methane transport (EoF_{CH_4}), or constant entropy production (EoEP). Table 6 shows that even though the imposition of EoEP or EoF_{CO_2} does not yield a minimum, it leads to a total entropy production which is not far from the optimum. Therefore, using EoEP as design guideline brings the total entropy production 90-98% towards the minimum in terms of the difference between the reference cases and the optimally controlled cases A-C. In the case of the EoF_{CO_2}, the total entropy production is brought up to 97-99% towards the minimum. This suggests that these two criteria can be used as relatively simple membrane design guidelines, when a reduction in the total entropy production is sought. Even though they are only approximations of the optimal solution, they are simple design criteria that make it possible to avoid elaborate optimization procedures. On the other hand, the use of EoF_{CH_4} does not reduce the entropy production significantly.

5.5. A practical realization of the findings

From a practical point of view, continuous control of the permeate partial pressures or permeate total pressure is not realistic. However, the optimal pressure profiles can be used as ideal limits for the practical design. For instance, practical control can be realized by dividing the membrane unit into a series of sub-units with different permeate pressures. Figure 7 shows the permeate pressure profile in the optimal counter-current case (solid line), and for a three-step approximation of it (dashed line). Compressors at the entrance of each sub-unit can be used to control the permeate pressure, as depicted in Fig. 8. With such a solution, the entropy production and, therefore, the lost work reduce by 5.3% with respect to the reference case. Since the total length of the unit is

This is the accepted version of an article published in Computers and Chemical Engineering
DOI: 10.1016/j.compchemeng.2018.06.002

the same as in the reference case, the investment costs due to membrane surface area are the same.

To add compressors to the membrane system means that the process requires additional power inputs, as well as additional costs for compressors. However, in most practical applications, the permeate gas needs either to be re-injected into the reservoir or to enter a second separation stage.

Under such circumstances, the permeate gas is typically re-compressed to pressures equal to that of the feed gas (or higher). In the present case, the compression ratio would be 50. Common industrial compressors have compression ratios of 2-4, and therefore, several compression stages are necessary. In the design phase, by choosing compressors with appropriate compression ratios and by relocating some compressors from downstream the separation process to in between the membrane stages, it is possible to optimally control the permeate pressure, without adding additional compressors to the global system, and therefore without adding capital costs.

To relocate the compressors that would be needed in a conventional process is a criterion that can also be used to choose the number of stages for the process. Indeed, since the entropy production reduces as the number of stages increases, the present approach cannot explicitly indicate the number of stages to be used in a specific application. However, the marginal entropy production decrement given by the introduction of an additional stage decreases rapidly: three stages already allow for 82% of the entropy production reduction obtained in the continuous case.

The control of the permeate pressure that is obtained by relocating the compressors results in 3.8% saving of the total power which is needed for re-compression, and, therefore, it decreases the operation costs. The location of the compressors (which is determined by the length of the membrane subunits) was in this case determined by considering equal length of the membrane subunits. This solution was suggested by the nearly linear permeate pressure profile obtained with the optimization procedure (Fig. 7). However, the lengths of the membrane subunits can also be used as additional parameters of the optimization procedure to find the optimal location of the compressors and further reduce the losses.

While the relocation of compressors of an existing membrane unit might be difficult to realize, it is easier to implement in the design phase, for units yet to be built.

In the present case the saving potential is small, but it would be higher for materials and designs with higher selectivities. With the use of a sweep gas with different compositions, it would also be possible to operate a step-wise control of gas partial pressures on the permeate side, and further improve the performance of the process.

Since the useful outputs, as well as the inputs, can be set as constraints of the optimization procedure, the minimization of entropy production can be done as a next step after maximization of the separation performances and preliminary economical considerations.

6. Conclusions

We have in this work presented a detailed method for minimization of the total entropy production of a membrane unit for CO_2 separation from natural gas using optimal control theory. The results of the analytical minimization method were verified

This is the accepted version of an article published in Computers and Chemical Engineering
DOI: 10.1016/j.compchemeng.2018.06.002

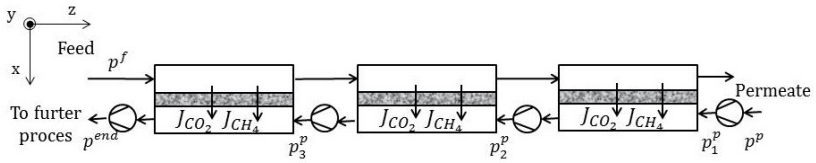

Figure 8: A schematic representation of an optimally controlled membrane unit, where the permeate gas is re-compressed for further processing. The optimal results are approximated by a three-step pressure profile. The pressure in every step is controlled by a compressor.

with a numerical minimization method. When we did not operate any control, the counter-current configuration was the one that led to the lowest entropy production.
When we controlled all the permeate partial pressures, the total entropy reduced by 38% with respect to the reference case, and the methane losses reduced to zero. The optimal results were characterized by constant entropy production and constant driving forces.
By controlling the total permeate pressure only, the entropy production decreased less (6.4% reduction in the counter-current configuration). Entropy production and driving forces were not constant in this case. However, the control of the total permeate pressure to impose constant entropy production or constant CO_2 driving force brought the entropy production very close to the minimum. This suggests that these two criteria can be used as design guidelines to reduce entropy production in CO_2 separation membranes. Moreover, membrane designs and materials with higher CO_2/methane selectivity would allow for a larger reduction of entropy production, when only the total pressure is controlled.
The theoretical optimal results can serve as limit for the practical design. A three-step permeate pressure profile that approximated the optimum was shown to reduce the entropy production by 5.3%. This caused 3.8% reduction in compressor power, when the permeate gas was re-compressed for further processing.

Acknowledgements

The project is funded by VISTA - a basic research program in collaboration with The Norwegian Academy of Science and Letters, and Statoil.

Appendix A. Deriving the local entropy production

In this appendix, we show the derivation of the entropy production of a membrane permeation process, from the entropy balance and the process conservation equations. The starting point is the entropy balance:

$$\begin{aligned} \Sigma_{irr} &= S^{out} - S^{in} + \int_0^L W\left(J_{CO_2} s^p_{CO_2} + J_{CH_4} s^p_{CH_4}\right) dz \\ &= \int_0^L \left(\frac{dS}{dz} + W\left(J_{CO_2} s^p_{CO_2} + J_{CH_4} s^p_{CH_4}\right)\right) dz \end{aligned} \tag{A.1}$$

This is the accepted version of an article published in Computers and Chemical Engineering
DOI: 10.1016/j.compchemeng.2018.06.002

where S is the entropy of the feed stream, and s_i is the molar entropy of the i component. From Eq. A.1, it is possible to recognize the entropy production:

$$\sigma = \frac{dS}{dz} + W\left(J_{CO_2} s^p_{CO_2} + J_{CH_4} s^p_{CH_4}\right) \tag{A.2}$$

Since the gas is considered to be ideal, the entropy of the stream can be written as:

$$\begin{aligned} S &= F_{CO_2} s_{CO_2} + F_{CH_4} s_{CH_4} \\ &= F_{CO_2}\left(s^{ref}_{CO_2} - R\ln\frac{x_{CO_2} p}{p^{ref}}\right) + F_{CH_4}\left(s^{ref}_{CH_4} - R\ln\frac{x_{CH_4} p}{p^{ref}}\right) \end{aligned} \tag{A.3}$$

where $s^{ref}_{CO_2}$ and $s^{ref}_{CH_4}$ are the reference molar entropy of CO_2 and methane respectively. Thus, the derivatives of the entropy with respect to the independent state variables are:

$$\left(\frac{\partial S}{\partial F_{CO_2}}\right)_{F_{CH_4}} = s_{CO_2} = s^{ref}_{CO_2} - R\ln\frac{x_{CO_2} p}{p^{ref}} \tag{A.4}$$

$$\left(\frac{\partial S}{\partial F_{CH_4}}\right)_{F_{CO_2}} = s_{CH_4} = s^{ref}_{CH_4} - R\ln\frac{x_{CH_4} p}{p^{ref}} \tag{A.5}$$

Substituting the partial derivatives of the entropy in Eq. A.2, we obtain:

$$\begin{aligned} \sigma &= \left(\frac{\partial S}{\partial F_{CO_2}}\right)_{F_{CH_4}} \frac{dF_{CO_2}}{dz} + \left(\frac{\partial S}{\partial F_{CH_4}}\right)_{F_{CO_2}} \frac{dF_{CH_4}}{dz} \\ &\quad + W\left(J_{CO_2} s^p_{CO_2} + J_{CH_4} s^p_{CH_4}\right) \\ &= s_{CO_2}\left(-W J_{CO_2}\right) + s_{CH_4}\left(-W J_{CH_4}\right) \\ &\quad + W\left(J_{CO_2} s^p_{CO_2} + J_{CH_4} s^p_{CH_4}\right) \\ &= W\left(J_{CO_2}\left(s^p_{CO_2} - s_{CO_2}\right) + J_{CH_4}\left(s^p_{CH_4} - s_{CH_4}\right)\right) \\ &= W\left(J_{CO_2}\left(-R\ln\frac{p^p_{CO_2}}{x_{CO_2} p}\right) + J_{CH_4}\left(-R\ln\frac{p^p_{CH_4}}{x_{CH_4} p}\right)\right) \\ &= W\left(J_{CO_2} X_{CO_2} + J_{CH_4} X_{CH_4}\right) \end{aligned} \tag{A.6}$$

which is the entropy production as given by Eq. 14.

Appendix B. Deriving the derivatives of the permeate mole fractions

Appendix B.1. Feed flow derivatives

The partial derivative of the permeate mole fractions with respect to the component feed flows have different expressions in different permeate flow configurations. In both co-current and counter-current configurations, the derivatives can be derived by differentiating Eq. 7. Even though the expressions for the permeate flows differ in the two

This is the accepted version of an article published in Computers and Chemical Engineering
DOI: 10.1016/j.compchemeng.2018.06.002

cases, by substituting Eq. 5 (for co-current) or Eq. 6 (for counter-current) into Eq. 7 and differentiating, we get:

$$\frac{\partial x^p_{CO_2}}{\partial F_{CO_2}} = \frac{\partial \left(F^p_{CO_2}/F^p\right)}{\partial F_{CO_2}} = -\frac{x^p_{CH_4}}{F^p} \tag{B.1}$$

$$\frac{\partial x^p_{CH_4}}{\partial F_{CO_2}} = \frac{\partial \left(1 - x^p_{CO_2}\right)}{\partial F_{CO_2}} = -\frac{\partial x^p_{CO_2}}{\partial F_{CO_2}} \tag{B.2}$$

Similarly, we get:

$$\frac{\partial x^p_{CO_2}}{\partial F_{CH_4}} = \frac{\partial \left(F^p_{CO_2}/F^p\right)}{\partial F_{CH_4}} = \frac{x^p_{CO_2}}{F^p} \tag{B.3}$$

$$\frac{\partial x^p_{CH_4}}{\partial F_{CH_4}} = \frac{\partial \left(1 - x^p_{CO_2}\right)}{\partial F_{CH_4}} = -\frac{\partial x^p_{CO_2}}{\partial F_{CH_4}} \tag{B.4}$$

In the cross-flow configuration, the derivatives can be derived by differentiating Eq. 8. We first rewrite Eq. 8 for the CO_2 mole fraction as:

$$x^p_{CO_2}\left(J_{CO_2} + J_{CH_4}\right) = J_{CO_2} \tag{B.5}$$

Substituting Eq. 11 in the expression above, and rewriting the methane mole fraction as $x^p_{CH_4} = 1 - x^p_{CO_2}$, we obtain:

$$x^p_{CO_2}\left(L_{CO_2} \ln \frac{x^p_{CO_2} p^p}{x_{CO_2} p} + L_{CH_4} \ln \frac{\left(1 - x^p_{CO_2}\right) p^p}{x_{CH_4} p}\right) = L_{CO_2} \ln \frac{x^p_{CO_2} p^p}{x_{CO_2} p} \tag{B.6}$$

Substituting Eq. 3 and carrying out the partial derivation with respect to F_{CO_2} on both sides of Eq. B.6, we obtain an expression for the CO_2 mole fraction:

$$\frac{\partial x^p_{CO_2}}{\partial F_{CO_2}} = x_{CH_4} \frac{\frac{x^p_{CO_2} L_{CH_4}}{F_{CH_4}} + \frac{x^p_{CH_4} L_{CO_2}}{F_{CO_2}}}{\frac{J}{R} + \frac{x^p_{CO_2} L_{CH_4}}{x^p_{CH_4}} + \frac{x^p_{CH_4} L_{CO_2}}{x^p_{CO_2}}} \tag{B.7}$$

The partial derivative of the methane mole fraction is:

$$\frac{\partial x^p_{CH_4}}{\partial F_{CO_2}} = \frac{\partial \left(1 - x^p_{CO_2}\right)}{\partial F_{CO_2}} = -\frac{\partial x^p_{CO_2}}{\partial F_{CO_2}} \tag{B.8}$$

Similarly, we can derive the partial derivatives of x^p_i with respect to the F_{CH_4}:

$$\frac{\partial x^p_{CO_2}}{\partial F_{CH_4}} = -x_{CO_2} \frac{\frac{x^p_{CO_2} L_{CH_4}}{F_{CH_4}} + \frac{x^p_{CH_4} L_{CO_2}}{F_{CO_2}}}{\frac{J}{R} + \frac{x^p_{CO_2} L_{CH_4}}{x^p_{CH_4}} + \frac{x^p_{CH_4} L_{CO_2}}{x^p_{CO_2}}} \tag{B.9}$$

$$\frac{\partial x^p_{CH_4}}{\partial F_{CH_4}} = -\frac{\partial x^p_{CO_2}}{\partial F_{CH_4}} \tag{B.10}$$

This is the accepted version of an article published in Computers and Chemical Engineering
DOI: 10.1016/j.compchemeng.2018.06.002

Appendix B.2. Permeate partial pressure derivatives

Carrying out the partial derivation with respect to p^p of both side of Eq. B.6, we obtain an expression for the CO_2 mole fraction:

$$\frac{\partial x^p_{CO_2}}{\partial p^p} = \frac{x^p_{CO_2} L_{CH_4} - x^p_{CH_4} L_{CO_2}}{p^p \left(\frac{J}{R} + \frac{x^p_{CO_2} L_{CH_4}}{x^p_{CH_4}} + \frac{x^p_{CH_4} L_{CO_2}}{x^p_{CO_2}} \right)} \tag{B.11}$$

The partial derivative of the methane mole fraction is:

$$\frac{\partial x^p_{CH_4}}{\partial p^p} = \frac{\partial \left(1 - x^p_{CO_2}\right)}{\partial p^p} = -\frac{\partial x^p_{CO_2}}{\partial p^p} \tag{B.12}$$

Appendix C. Numerical solution of the problem

Section 3.3 presented the conditions that are necessary for a local minimum in the objective function. Since several local minima may exist, and the minimum found in calculations might not correspond to the global minimum, we compared the results found with the analytical procedure presented in Section 3.3 with those obtained by solving the minimization problem numerically. We used the Matlab optimization function "fmincon", which finds the minimum of an objective function subject to equality and inequality constraints, by using a sequential quadratic programming method.
The objective function is the total entropy production, which is expressed as a function of the state and control variables.
The equality constraints for the numerical problem are given by the inlet boundary conditions ($F_i(z = 0) = F_i^{in}$), by the constraint on the duty of the membrane system (Eq. 40), and by the governing equations (Eqs. 2). For the numerical solution, it is necessary to transform the differential Eqs. 2 into algebraic equations. Therefore, the term on the left-hand side of the two governing equations is approximated on a spatial grid of $n = 100$ points, using a finite difference method. Thus, the two differential equations turn into two systems of n algebraic equations, that are used as equality constraints for the minimization problem.
The inequality constraints are represented by the state inequality constraints (Eq. 18).
As for the analytical case, solving the minimization problem numerically does not guarantee that the minimum that we found is the global minimum. Therefore, we carried out the same numerical calculations several times, with different random initial profiles for the state and control variables. For all instances, the numerical and analytical solutions were found to agree with a relative accuracy of the order of the numerical accuracy of the calculations (10^{-5}).

Appendix D. Ideal compression power

When the permeate gas is injected into the reservoir or it needs to go through a further separation stage, the permeate gas needs to be re-compressed to a certain pressure,

This is the accepted version of an article published in Computers and Chemical Engineering
DOI: 10.1016/j.compchemeng.2018.06.002

p^{end}. If we assume the compression isothermal and reversible and the gas ideal, the power necessary for the compression is:

$$W_{compr} = -F^{p,out} \int_{p^p}^{p^{end}} pdv = F^{p,out} RT \ln \frac{p^{end}}{p^p} \tag{D.1}$$

where $F^{p,out}$ is the permeate flow leaving the membrane unit and v is the specific volume. We choose to use the ideal compression power in calculations because the compressor efficiency is not object of this study.

References

[1] R. W. Baker, B. T. Low, Gas separation membrane materials: a perspective, Macromolecules 47 (20) (2014) 6999–7013.

[2] P. Bernardo, E. Drioli, G. Golemme, Membrane gas separation: a review/state of the art, Industrial & Engineering Chemistry Research 48 (10) (2009) 4638–4663.

[3] S. Mokhatab, W. A. Poe, Handbook of natural gas transmission and processing, Gulf Professional Publishing, Oxford, United Kingdom, 2012.

[4] L. Peters, A. Hussain, M. Follmann, T. Melin, M.-B. Hägg, CO_2 removal from natural gas by employing amine absorption and membrane technology - a technical and economical analysis, Chemical Engineering Journal 172 (2) (2011) 952–960.

[5] S. Stern, J. Perrin, E. Naimon, Recycle and multimembrane permeators for gas separations, Journal of membrane science 20 (1) (1984) 25–43.

[6] Y. Huang, T. C. Merkel, R. W. Baker, Pressure ratio and its impact on membrane gas separation processes, Journal of Membrane Science 463 (2014) 33–40.

[7] B. D. Bhide, S. A. Stern, Membrane processes for the removal of acid gases from natural gas. I. process configurations and optimization of operating conditions, Journal of Membrane Science 81 (3) (1993) 209–237.

[8] R. Qi, M. Henson, Optimization-based design of spiral-wound membrane systems for CO_2/ CH_4 separations, Separation and Purification Technology 13 (3) (1998) 209–225.

[9] S. Tessendorf, R. Gani, M. L. Michelsen, Modeling, simulation and optimization of membrane-based gas separation systems, Chemical Engineering Science 54 (7) (1999) 943–955.

[10] J. Hao, P. Rice, S. Stern, Upgrading low-quality natural gas with H_2S- and CO_2-selective polymer membranes: Part I. Process design and economics of membrane stages without recycle streams, Journal of Membrane Science 209 (1) (2002) 177–206.

This is the accepted version of an article published in Computers and Chemical Engineering
DOI: 10.1016/j.compchemeng.2018.06.002

[11] H. Chang, W.-C. Hou, Optimization of membrane gas separation systems using genetic algorithm, Chemical Engineering Science 61 (16) (2006) 5355–5368.

[12] J. Hao, P. Rice, S. Stern, Upgrading low-quality natural gas with H_2S- and CO_2-selective polymer membranes: Part II. Process design, economics, and sensitivity study of membrane stages with recycle streams, Journal of Membrane Science 320 (1) (2008) 108–122.

[13] M. Safari, A. Ghanizadeh, M. M. Montazer-Rahmati, Optimization of membrane-based CO_2-removal from natural gas using simple models considering both pressure and temperature effects, International Journal of Greenhouse Gas Control 3 (1) (2009) 3–10.

[14] M. Scholz, M. Alders, T. Lohaus, M. Wessling, Structural optimization of membrane-based biogas upgrading processes, Journal of Membrane Science 474 (2015) 1–10.

[15] J. Xu, R. Agrawal, Membrane separation process analysis and design strategies based on thermodynamic efficiency of permeation, Chemical engineering science 51 (3) (1996) 365–385.

[16] J. Perrin, S. Stern, Modeling of permeators with two different types of polymer membranes, AIChE journal 31 (7) (1985) 1167–1177.

[17] J. Carl, D. Fedor, Tracking global carbon revenues: A survey of carbon taxes versus cap-and-trade in the real world, Energy Policy 96 (2016) 50–77.

[18] G. Gouy, Sur l'énergie utilisable, Journal de Physique 8 (1889) 501–518.

[19] M. Pavelka, V. Klika, P. Vagner, F. Marsik, Generalization of exergy analysis, Applied Energy 137 (2015) 158 – 172.

[20] B. Andresen, J. Gordon, Optimal heating and cooling strategies for heat exchanger design, Journal of Applied Physics 71 (1) (1992) 76–79.

[21] P. Salamon, J. D. Nulton, G. Siragusa, A. Limon, D. Bedeaux, S. Kjelstrup, A simple example of control to minimize entropy production, Journal of Non-Equilibrium Thermodynamics 27 (1) (2002) 45–55.

[22] E. Johannessen, L. Nummedal, S. Kjelstrup, Minimizing the entropy production in heat exchange, International Journal of Heat and Mass Transfer 45 (13) (2002) 2649–2654.

[23] P. Lerou, T. Veenstra, J. Burger, H. Ter Brake, H. Rogalla, Optimization of counterflow heat exchanger geometry through minimization of entropy generation, Cryogenics 45 (10) (2005) 659–669.

[24] L. Nummedal, S. Kjelstrup, Equipartition of forces as a lower bound on the entropy production in heat exchange, International Journal of Heat and Mass Transfer 44 (15) (2001) 2827 – 2833.

This is the accepted version of an article published in Computers and Chemical Engineering
DOI: 10.1016/j.compchemeng.2018.06.002

[25] E. Johannessen, S. Kjelstrup, Minimum entropy production rate in plug flow reactors: an optimal control problem solved for SO_2 oxidation, Energy 29 (12) (2004) 2403–2423.

[26] E. Johannessen, S. Kjelstrup, A highway in state space for reactors with minimum entropy production, Chemical Engineering Science 60 (12) (2005) 3347–3361.

[27] Ø. Wilhelmsen, E. Johannessen, S. Kjelstrup, Energy efficient reactor design simplified by second law analysis, International Journal of Hydrogen Energy 35 (24) (2010) 13219 – 13231.

[28] O. C. Mullins, R. S. Berry, Minimization of entropy production in distillation, The Journal of Physical Chemistry 88 (4) (1984) 723–728.

[29] S. K. Ratkje, E. Sauar, E. M. Hansen, K. M. Lien, B. Hafskjold, Analysis of entropy production rates for design of distillation columns, Industrial & Engineering Chemistry Research 34 (9) (1995) 3001–3007.

[30] P. Salamon, J. D. Nulton, The geometry of separation processes: A horse-carrot theorem for steady flow systems, Europhysics Letters 42 (5) (1998) 571–576.

[31] B. Andresen, P. Salamon, Distillation by thermodynamic geometry, in: Thermodynamics of energy conversion and transport, Springer, 2000, pp. 319–331.

[32] G. M. de Koeijer, S. Kjelstrup, Minimizing entropy production rate in binary tray distillation, International Journal of Thermodynamics 3 (3) (2000) 105–110.

[33] L. Shu, L. Chen, F. Sun, Performance optimization of a diabatic distillation-column by allocating a sequential heat-exchanger inventory, Applied Energy 84 (9) (2007) 893 – 903.

[34] E. Johannessen, A. Røsjorde, Equipartition of entropy production as an approximation to the state of minimum entropy production in diabatic distillation, Energy 32 (4) (2007) 467–473.

[35] A. Mourgues, J. Sanchez, Theoretical analysis of concentration polarization in membrane modules for gas separation with feed inside the hollow-fibers, Journal of Membrane Science 252 (1) (2005) 133–144.

[36] W. Echt, P. Meister, Design, fabrication and startup of an offshore membrane CO_2 removal system, in: 88^{th} Annual Convention-UOP LLC. Gas Processors Association, 2009.

[37] A. Lee, H. Feldkirchner, S. Stern, A. Houde, J. Gamez, H. Meyer, Field tests of membrane modules for the separation of carbon dioxide from low-quality natural gas, Gas Separation & Purification 9 (1) (1995) 35–43.

[38] E. Magnanelli, Ø. Wilhelmsen, E. Johannessen, S. Kjelstrup, Enhancing the understanding of heat and mass transport through a cellulose acetate membrane for CO_2 separation, Journal of Membrane Science 513 (2016) 129 – 139.

This is the accepted version of an article published in Computers and Chemical Engineering
DOI: 10.1016/j.compchemeng.2018.06.002

[39] D. Coker, T. Allen, B. Freeman, G. Fleming, Nonisothermal model for gas separation hollow-fiber membranes, AIChE journal 45 (7) (1999) 1451–1468.

[40] S. S. Hosseini, S. Najari, P. K. Kundu, N. R. Tan, S. M. Roodashti, Simulation and sensitivity analysis of transport in asymmetric hollow fiber membrane permeators for air separation, RSC Advances 5 (105) (2015) 86359–86370.

[41] A. Brunetti, F. Scura, G. Barbieri, E. Drioli, Membrane technologies for co2 separation, Journal of Membrane Science 359 (1-2) (2010) 115–125.

[42] S. Kjelstrup, D. Bedeaux, Non-equilibrium thermodynamics of heterogeneous systems, Vol. 16, World Scientific, Singapore, 2008.

[43] R. W. Baker, K. Lokhandwala, Natural gas processing with membranes: an overview, Industrial & Engineering Chemistry Research 47 (7) (2008) 2109–2121.

[44] M. D. Donohue, B. S. Minhas, S. Y. Lee, Permeation behavior of carbon dioxide-methane mixtures in cellulose acetate membranes, Journal of Membrane Science 42 (3) (1989) 197–214.

[45] A. E. Bryson, Applied optimal control: optimization, estimation and control, CRC Press, Boca Raton, Florida, 1975.

[46] D. E. Kirk, Optimal control theory: an introduction, Courier Corporation, San José, California, 2012.

[47] R. W. Baker, Future directions of membrane gas separation technology, Industrial & Engineering Chemistry Research 41 (6) (2002) 1393–1411.

[48] S. Amelkin, A. Tsirlin, J. Burzler, S. Schubert, K.-H. Hoffmann, Minimal work for separation processes of binary mixtures, Open Systems & Information Dynamics 10 (04) (2003) 335–349.

This is the accepted version of an article published in Computers and Chemical Engineering
DOI: 10.1016/j.compchemeng.2018.06.002